Self-Association Process of a Peptide in Solution: From β-Sheet Filaments to Large Embedded Nanotubes

C. Valéry,*§ F. Artzner,* B. Robert,† T. Gulick,‡ G. Keller,* C. Grabielle-Madelmont,* M.-L. Torres,§ R. Cherif-Cheikh,§ and M. Paternostre†

*Unité Mixte de Recherche Centre National de la Recherche Scientifique 8612, Faculté de Pharmacie, Châtenay-Malabry, France; †Unité de Recherche Associée 2096 Centre National de la Recherche Scientifique-Commissariat à l'Energie Atomique, Département de Biologie Joliot Curie/Service de Biophysique des Fonctions Membranaires, Commissariat à l'Energie Atomique-Saclay, France; ‡Centre de Génétique Moléculaire Centre National de la Recherche Scientifique, Gif sur Yvette, France; and §Ipsen Pharma SA, Sant Feliu de Llobregat, Barcelona, Spain

ABSTRACT Lanreotide is a synthetic octapeptide used in the therapy against acromegaly. When mixed with pure water at 10% (w/w), Lanreotide (acetate salt) forms liquid crystalline and monodisperse nanotubes with a radius of 120 Å. The molecular and supramolecular organization of these structures has been determined in a previous work as relying on the lateral association of 26 β-sheet filaments made of peptide noncovalent dimers, the basic building blocks. The work presented here has been devoted to the corresponding self-association mechanisms, through the characterization of the Lanreotide structures formed in water, as a function of peptide (acetate salt) concentration (from 2% to 70% (w/w)) and temperature (from 15°C to 70°C). The corresponding states of water were also identified and quantified from the thermal behavior of water in the Lanreotide mixtures. At room temperature and below 3% (w/w) Lanreotide acetate in water, soluble aggregates were detected. From 3% to 20% (w/w) long individual and monodisperse nanotubes crystallized in a hexagonal lattice were evidenced. Their molecular and supramolecular organizations are identical to the ones characterized for the 10% (w/w) sample. Heating induces the dissolution of the nanotubes into soluble aggregates of the same structural characteristics as the room temperature ones. The solubilization temperature increases from 20°C to 70°C with the peptide concentration and reaches a plateau between 15% and 25% (w/w) in peptide. These aggregates are proposed to be the β-sheet filaments that self-associate to build the walls of the nanotubes. Above 20% (w/w) of Lanreotide acetate in water, polydisperse embedded nanotubes are formed and the hexagonal lattice is lost. These embedded nanotubes exhibit the same molecular and supramolecular organizations as the individual monodisperse nanotubes formed at lower peptide concentration. The embedded nanotubes do not melt in the range of temperature studied indicating a higher thermodynamic stability than individual nanotubes. In parallel, the thermal behaviors of water in mixtures containing 2–80% (w/w) in peptide have been studied by differential scanning calorimetry, and three different types of water were characterized: 1), bulk water melting at 0°C, 2), nonfreezing water, and 3), interfacial water melting below 0°C. The domains of existence and coexistence of these different water states are related to the different Lanreotide supramolecular structures. All these results were compiled into a binary Lanreotide-water phase diagram and allowed to propose a self-association mechanism of Lanreotide filaments into monodisperse individual nanotubes and embedded nanotubes.

INTRODUCTION

Lanreotide, a synthetic analog of natural somatostatin, is an octapeptide used in the treatment of acromegaly. A concentrated Lanreotide acetate (Lan-ac) hydrogel (30% (w/w), Autogel, Barcelona, Spain) exhibits remarkable controlled and sustained release properties when used as a subcutaneous implant (Cherif-Cheikh et al., 1998). For poorly stable therapeutic compounds such as peptides, such a pharmacokinetic profile is a challenging property that is looked for. In this domain of research, the simplicity of Lanreotide hydrogels is noteworthy when compared to sophisticated delivery systems such as liposomes or polymeric nanoparticles (Banakar, 1997; Langer, 2001). The simplicity of the Lanreotide gel formulation together with its remarkable pharmacokinetic properties raised the question of the self-associating structures formed by Lanreotide in water.

Molecular self-assembly can be defined as the spontaneous process of generation of supramolecular structures through intermolecular noncovalent interactions. Monitoring self-assembly makes the design of programmed systems and the corresponding new ordered materials possible (Lehn, 2002; Whitesides and Boncheva, 2002; Hartgerink et al., 2002). Self-assembly is also relevant in life science, with the numerous complex self-organized functional systems encountered. Understanding the basic principles generating this phenomenon should lead to a better knowledge of biological processes (Klug, 1983) and to the conception of new biomimetic nanomaterials (Zhang, 2003). In the specific case of self-organized tubular architectures based on proteins and peptides, nature provides a variety of examples of such structures, from virus capsids (Klug, 1983), microtubules (Nogales et al., 1998), and actin filaments (Holmes et al., 1990) to amyloid fibrils made of pathological misfolded proteins (Serpell, 2000). The investigation of the self-association processes involved in the generation of proteins

Submitted September 26, 2003, and accepted for publication December 8, 2003.

Address reprint requests to Maïté Paternostre, URA 2096 CNRS-CEA, DBJC/SBFM, Laboratoire des protéines transductrices d'énergie, Bât. 528, CEA-Saclay, F-91191 Saclay, France. Tel.: 33-(0)1-69-08-67-49; Fax: 33-(0)1-69-08-43-89; E-mail: maite.paternostre@cea.fr.

0006-3495/04/04/2484/18 $2.00

and peptides fibers is therefore an important general feature that opens the door to a wide set of applications.

We have recently shown that Lanreotide (acetate salt) at 10% (w/w) in pure water spontaneously forms noteworthy monodisperse liquid crystalline nanotubes with a radius of 120 Å (Valéry et al., 2003). The originality of Lanreotide nanotubes firstly comes from the order of magnitude of their radius, which is comparable to biological tubular self-assemblies such as the capsid of the tobacco mosaic virus (Klug, 1983; Namba and Stubbs, 1986) or microtubules (Hitt et al., 1990; Nogales, 1998; Nogales and Inclan, 2000). Whereas these structures are formed by polypeptides of high molecular weight, Lanreotide is a small peptide of eight residues. Some self-assembling systems based on synthetic peptides and biomimetic principles also exhibit the tubular symmetry. For instance, cyclic D,L-peptides of less than ten residues form long tubular architectures by self-assembly of the disc-like molecules, through one-dimensional intermolecular β-sheet hydrogen bonds (Ghadiri et al., 1993; Bong et al., 2001). However, the diameter of these tubes is defined by the molecular size of the basic peptide building block and thus limited to the nanometer scale. However, Vauthey et al. (2002) showed that amphiphilic peptides designed as polar lipids with a hydrophilic head and hydrophobic tail form vesicles and micelles at low concentration in water but also large nanotubes with an average diameter of 30–50 nm. Designed rod-shaped chiral peptides of similar molecular size self-assemble in water into a hierarchy of twisted supramolecular structures, from ribbons to 8-nm width long fibers (Aggeli et al., 2001). The larger Lanreotide nanotubes also exhibit a hierarchical organization within their walls: they are constituted by the lateral association of 26 β-sheet filaments. The building block of the filaments is a Lanreotide noncovalent dimer, which is stabilized by hydrophobic effect and electrostatic repulsion between β-hairpin peptides. The stacking of these dimers generates the filaments, through the formation of hydrogen bonds in antiparallel β-sheet networks. This hierarchy, the peculiar symmetries and interactions involved in the self-organization of Lanreotide, can be compared with the characteristic properties of the amyloid β-peptide fibers. Both organizations rely on an antiparallel β-sheet organization of a β-hairpin peptide into hierarchical assemblies and on the importance of highly hydrophobic residues for the nucleation process (Gazit, 2002; Serpell, 2000). Therefore Lanreotide appears as a new model peptide to investigate general protein-like molecular self-assembly processes leading to well-organized fibers and nanotubes.

The experiments presented here were devoted to the investigation of the molecular and supramolecular mechanisms involved in the formation of the peculiar Lanreotide hydrogels. To understand the self-assembly of Lanreotide, a phase diagram approach has been adopted. The Lanreotide-water system has been examined over a wide range of concentrations (2–70%) and temperatures (10–70°C). A variety of physicochemical techniques were used to determine the characteristics and the domains of existence of the different structures formed by the peptide in water. The macroscopic scale was investigated by light scattering and optical microscopy, the supramolecular scale by electron microscopy and small angle x-ray scattering (SAXS), and the molecular scale by vibrational spectroscopic techniques (Fourier transform infrared (FTIR) and FT-Raman). The second component of the system, water in the mixtures, was investigated by differential scanning calorimetry. It was found that at low concentrations of peptide, β-sheet filaments were formed as soluble precursors of the nanotubes present at higher concentrations. Two types of tubular structures were characterized as a function of Lanreotide concentration, i.e., individual and embedded nanotubes, the latest being found thermodynamically more stable than the individual nanotubes. From these results, we propose a model for the mechanism of formation of the Lanreotide individual and embedded nanotubes.

MATERIALS AND METHODS

Materials

Lanreotide acetate powder was obtained from Ipsen Pharma (Barcelona, Spain). The Lanreotide molecule was synthesized by a Kinerton batch process (Dublin, Ireland), which includes a flash-freeze lyophilization. Glycerol 99.9%, solid naphthalene 99%, and β-mercaptoethanol 14 M were purchased from Sigma (Paris, France).

Samples preparation

The Lanreotide acetate aqueous solutions up to 10% (w/w) were prepared by adding deionized water to a weighed fraction of Lanreotide acetate powder. For concentrations higher than 10% (w/w), the viscosity of the mixtures required the application of a special mixing technique. The system used consists in two plastic syringes of 2 mL connected by a small tap. Both syringes were filled with a weighed fraction of, respectively, Lanreotide acetate powder and water. The syringe containing the peptide was connected to the tap and air vacuum was performed with a water pump. The other syringe was then connected to the tap and the mixture realized by passing the dispersion from a syringe to the other until total homogenization. The samples were prepared at least 24 h before the experiments and stored at 4°C.

Optical microscopy

Optical microscopy experiments were realized at room temperature (~20°C) with crossed polarizers or phase contrast using a type 120 Nikon microscope (Tokyo, Japan) equipped with a Nikon 20× objective. The photographs were obtained with a digital camera, Nikon Coolpix 950. The samples observed were conditioned either in 1.3-mm glass capillaries or between glass slices.

Turbidity measurements

The evolution of the Lanreotide acetate samples turbidity was investigated as a function of concentration on a Perkin-Elmer double beam spectrophotometer (Lambda 2; Foster City, CA). The optical density at 500 nm was recorded during the continuous addition of a Lanreotide acetate solution

from a syringe into a cuvette containing an initial weighed volume of 1.5 mL of deionized water maintained under magnetic stirring, as previously described (Paternostre et al., 1997; Pott et al., 1998). A syringe pump monitored the constant addition rate of the initial Lanreotide acetate solution of 6% (w/w) in pure water. To reach a final concentration of 5% (w/w), four successive additions of 1 mL Lanreotide acetate at 6% (w/w) at a rate of 1 mL/36 min were performed to an initial volume of 1.5 mL. In between each addition, 1 mL of the solution was removed from the cuvette to allow the next 1 mL to fill the cuvette. This experiment was possible, because within the time of the experiment the solution at 6% (w/w) in the syringe remains liquid. Indeed, at this concentration, the formation of the peptide gel takes few hours. This rate control allowed the calculation of the Lanreotide acetate concentration in the cuvette at a time t from the known concentration in the syringe and from the initial volume of water, using Eq. 1:

$$[\mathrm{Lan}]_t = ([\mathrm{Lan}]_s \times r_s \times t)/(V_0 + r_s \times t), \quad (1)$$

where $[\mathrm{Lan}]_t$ and $[\mathrm{Lan}]_s$ (% w/w) are, respectively, the Lanreotide acetate concentrations in the cuvette at the time t and in the syringe, V_0 is the initial volume of water in the cuvette, r_s is (mL/s) the addition rate of the Lanreotide acetate solution from the syringe into the cuvette, and t (s) is the time of measurement.

Very small and small angle x-ray scattering

Very small angle x-ray scattering (VSAXS) and small angle x-ray scattering (SAXS) were performed on the high brilliance ID2A beamline of the European Synchrotron Radiation Facility (ESRF, Grenoble, France). Distinct ranges of sample-detector distances were applied for the VSAXS and the SAXS experiments, respectively, from 5.6 m and 1.4 m to 1.5 m depending on the experiments. The x-ray patterns were therefore recorded for two ranges of reciprocal spacing $q(\text{Å}^{-1})$ from 0.01 Å^{-1} to 0.12 Å^{-1} and from 0.02 Å^{-1} to 0.5 Å^{-1}, respectively. The samples were conditioned in 1.2–1.3-mm glass capillaries and introduced into a homemade capillaries holder, which allows maintaining 20 capillaries all together at a controlled temperature or applying a determined temperature program monitored via a computer. The x-ray patterns were detected and recorded via a CCD (chip charge-coupled device) camera detector. All samples exhibited powder diffraction and the scattering intensities as a function of the radial wave vector, $q = 4\pi/\lambda \times \sin(\theta)$, were determined by circular integration (Narayanan et al., 2001).

Sample preparation and electron microscopy

The samples were prepared in the presence of 30% (w/w) dried glycerol as cryoprotectant. As a preliminary, it was verified that the presence of glycerol did not affect the supramolecular structures formed by Lanreotide, using optical microscopy, SAXS, and wide angle x-ray scattering (WAXS) (data not shown). A droplet of sample was deposited on a copper holder and then dropped into liquid propane and stored in liquid nitrogen until replication. The samples were fractured under vacuum (less than 5×10^{-7} Torr) with a liquid nitrogen-cooled knife in a Balzers BAF 301 apparatus equipped with an electron gun for platinum shadowing. In the case of freeze-etching, the samples were etched before shadowing to increase their relief. The two kinds of replicas obtained were examined with a Philips (Eindhoven, The Netherlands) 301 electron microscope.

Fourier transform infrared spectroscopy

Attenuated total reflectance (ATR) FTIR spectra were measured at 4 cm^{-1} resolution with a Bruker (Billerica, MA) IFS 66 spectrophotometer equipped with a 45° n ZnSe ATR attachment. The spectra shown resulted from the average of 50 scans. Spectra were corrected for the linear dependence on the wavelength of the absorption measured by ATR. The water signal was removed by a subtraction of pure water spectrum recorded the day of the experiment. Analysis of the Lanreotide conformation was performed by deconvolution of the absorption spectra, either as a sum of Gaussian components (Byler and Susi, 1986) or as a sum of spectra assigned to different structures (Venyaminov and Kalnin, 1990).

Fourier transform-Raman spectroscopy

Fourier transform-Raman spectra were recorded at 4 cm^{-1} resolution using a Bruker IFS 66 interferometer coupled to a Bruker FRA 106 Raman module equipped with a continuous Nd:YAG laser providing excitation at 1064 nm as described in Mattioli et al. (1994). All spectra were recorded at room temperature with backscattering geometry from concentrated samples (over 10% (w/w) of Lanreotide acetate) held in standard aluminum cups. The spectra resulted from 1000 to 10,000 coadded interferograms depending on the samples signal.

Differential scanning calorimetry

Calorimetry experiments were performed using a Perkin-Elmer DSC7 calorimeter with samples conditioned into 40-μL aluminum pans (Perkin-Elmer Model B014-3031), the samples weight varying between 5 mg and 2 mg. The crystallization curves were recorded at 5°C/min from 20°C to −80°C and the melting curves at 2°C/min from −80°C to 20°C. Highly purified lauric acid and pure water were used to calibrate the calorimeter for temperature and quantitative heat determination.

To cover a large range of concentrations and to ensure the continuity of the experiments, a special procedure was used to control the water content of the samples. For each initial Lanreotide acetate concentration, two very small holes (less than 0.2 mm) were made in the pan cover after the pan sealing by an especially sharp pin (Cansell et al., 1991). The pans were weighed before and after each DSC recording. No detectable water evaporation was measured after the temperature cycle. The water content was decreased between two recordings by heating the pans at 30°C. After this heating, each pan was weighed, allowing the quantification of the water content decrease, considering that the initial Lanreotide acetate mass introduced in the pan remains constant. This special procedure allows measuring the thermal behavior of mixtures from 0.5% up to 85% (w/w) of Lanreotide acetate in water. The transition enthalpies were calculated using the samples weights measured just before the experiments.

A graphical analysis of the melting curves was performed (Fig. 12 *c*). When the melting of the frozen water entirely occurs at 0°C and the onset temperature of the transition, T_{on}, was taken at the intersection of the tangent to the left side of the DSC curve with the baseline. In this case, pure water was used as standard for temperature and enthalpy change determination.

Some of the melting curves obtained from Lanreotide acetate/water mixtures show a fraction of water melting below 0°C together with or without water melting at 0°C, i.e., bulk water. To determine the contribution of each type of water, the melting curves were graphically treated as the following (Fig. 12 *c*): point A on the melting curve determining the T_{on} of the water melting below 0°C was graphically determined as described above for the water melting at 0°C, and point B corresponds to 0°C. The peak relative to the frozen water fraction melting below 0°C was defined by the area ABC, the line BC being drawn from 0°C parallel to DE, assuming the same down curve shape for both water types. The area BDEC depicts the melting of the bulk frozen water. The respective areas under both peaks were determined by weighing. The transition enthalpy change (ΔH_{bulk}) corresponding to the area BDEC was deduced from that of pure ice melting (333 J/g). When frozen water melts below 0°C, its enthalpy change ($\Delta H_{<0°C}$) is lower than that of pure ice and decreases with decreasing temperature (Franks, 1982a; Privalov, 1980). Franks (1982a) has proposed a law for the dependence of $\Delta H_{<0°C}$ on temperature: $\Delta H = 387.7 + 56.24 \times \exp(-T/35.2)$. Therefore, the experimental $\Delta H_{<0°C}$ have been corrected by

using this empirical law. A mean temperature (T^* in Fig. 12 *c*) was determined for the water melting below 0°C as the intersection of the tangent to the left side of the curve with the baseline. In a first approximation, this temperature value was considered as the mean $\Delta H_{<0°C}$ standard for the frozen water melting corresponding to the area ABC of the DSC curve.

RESULTS

Determination of the different concentration domains of the phase diagram at 20°C

In the concentration range examined by electron microscopy (from 2% to 30% (w/w) of Lanreotide acetate), evidences were obtained in favor of three types of Lanreotide acetate behavior in water (Fig. 1).

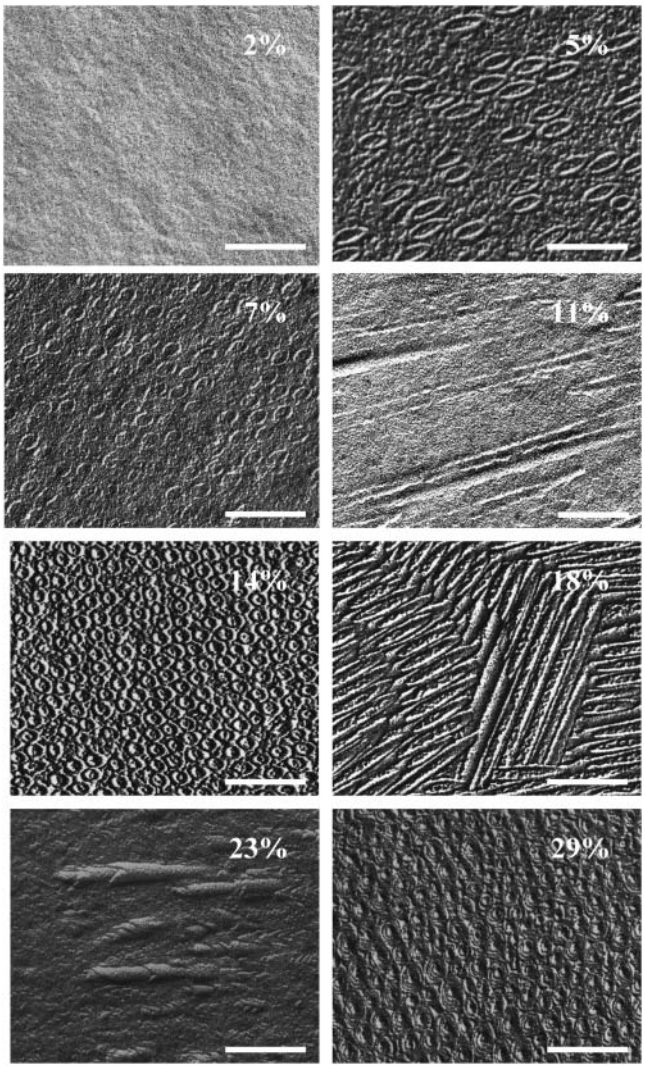

FIGURE 1 Electron micrographs of replicas of Lanreotide acetate in water mixtures after freeze-fracture (2%, 7%, 11%, and 23% (w/w) of Lanreotide acetate) and freeze-etching (5%, 14%, 18%, and 29% (w/w) of Lanreotide acetate). The corresponding concentrations of Lanreotide acetate (% w/w in water) are indicated on each micrograph. The scale bar corresponds to 100 nm.

1. For 2% (w/w) of Lanreotide acetate in water, no structure could be visualized on the electron micrographs (Fig. 1).
2. For Lanreotide acetate concentrations ranging from 5% to 20% (w/w), long nanotubes were observed (Fig. 1), the increase of peptide concentration inducing an increase of the density of the structures. The transversal cuts allowed to measure an average radius of ~120 Å, independently of peptide concentration. A short distance order could be visualized in all the micrographs, i.e., parallel organization of the nanotubes in their close vicinity. Local hexagonal networks can be observed, particularly well defined on the electron micrograph of the 14% (w/w) mixture. All the longitudinal cuts exhibit similar hollow tubular sections of individual objects. Their absolute length could not be determined because of the cut performed by the freeze-fracture technique, which generated incomplete tubes. Nevertheless the maximal length measured on the micrographs reaches 1 μm. In this entire concentration range, the morphology of the objects revealed by electron microscopy is similar to the one characterized by Valéry et al. (2003) for a 10% (w/w) Lanreotide acetate in water mixture. The molecular and the supramolecular arrangements of the peptide within the nanotubes have been resolved for this specific concentration.
3. For Lanreotide acetate concentration over 20% (w/w) in water, another morphology of tubular objects is evidenced. The transversal cuts of these structures show three to four concentric circular sections without any continuity between their walls contrary to cochlaete cylinders-like objects (Archibald and Yager, 1992). These views suggest a compact embodiment of individual nanotubes. The longitudinal cuts exhibit hollow tubular sections with several tubes fitting one into another supporting the embedded nanotubes morphology. As for lower Lanreotide concentrations, the average length of the tubular objects could not be measured because of the cut performed by the freeze-fracture technique. However these objects appear shorter and less flexible than the single nanotubes observed under 20% w/w.

The Lanreotide behavior was separately studied in these three concentration domains using a variety of techniques, at room temperature and as a function of temperature.

Lanreotide behavior below 3% (w/w) and at room temperature

The turbidity at 500 nm was recorded as a function of Lanreotide acetate concentration up to 5.5% (w/w) in water (Fig. 2). The turbidity curve is linear until 2.8% (Fig. 2, *inset*), concentration at which an abrupt breakpoint is recorded that can be directly associated with an aggregation phenomenon. Over this limited concentration range, gelation of the Lanreotide acetate aqueous mixtures occurs after a few

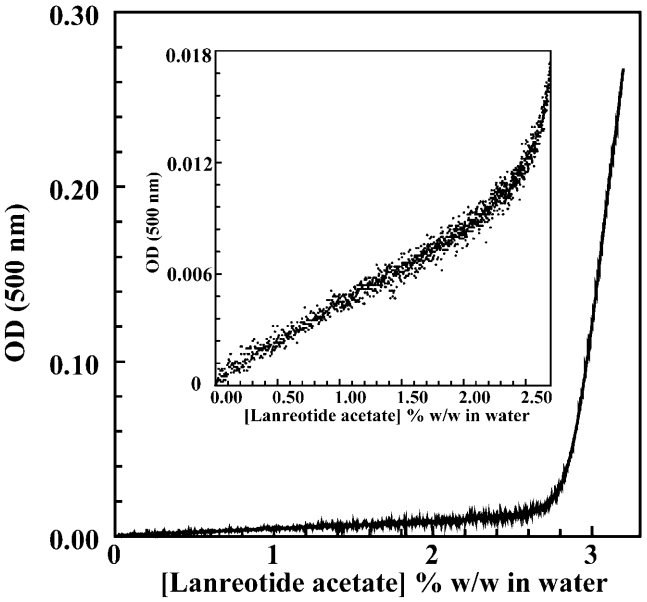

FIGURE 2 Evolution of Lanreotide-water mixtures optical density at 500 nm and 20°C upon continuous addition of Lanreotide acetate in water up to 5.5% w/w. (*Inset*) Zoom on optical density evolution for low peptide concentration.

hours. This macroscopic phenomenon is directly correlated to the occurrence of birefringence in the mixtures.

From a structural point of view, neither VSAXS patterns nor electron micrographs obtained for a 2% (w/w) Lanreotide acetate aqueous solution show the presence of detectable organization (data not shown). However, the SAXS pattern relative to this same concentration exhibits a weak and broad central scattering at ~0.1 $Å^{-1}$ (60 Å) that can be generated by either large anisotropic aggregates with a characteristic size of ~60 Å or small aggregates interacting at a distance of 60 Å (Fig. 3 *a*). This result however demonstrates the presence of aggregates at this low peptide concentration domain. The apparent discrepancy between electron microscopy (absence of detectable objects) and SAXS (presence of scattering objects) observations is possibly due to either the low peptide concentration, i.e., the small number of scattering objects would not be visible on the electron micrograph, or a size of the aggregates under the resolution of the electron microscopy technique (estimated resolution of the electron microscopy technique: 20 Å).

The FTIR spectrum recorded for 2% (w/w) of Lanreotide acetate in water (Fig. 3 *b*) exhibits four distinct vibrations in the frequency range of the amide I mode (1600–1700 cm^{-1}). In agreement with the literature (Krimm and Bandekar, 1986; Bandekar, 1992; Goormaghtigh et al., 1994; Haris and Chapman, 1995), these vibrations can be assigned to backbone carbonyl groups involved in hydrogen bonds in an antiparallel β-sheet (1620 cm^{-1} and 1685 cm^{-1}), in turn (1670 cm^{-1}) and in random (1635 cm^{-1}) conformations, respectively. Besides the relatively high contribution of the random conformation, this spectrum demonstrates that the

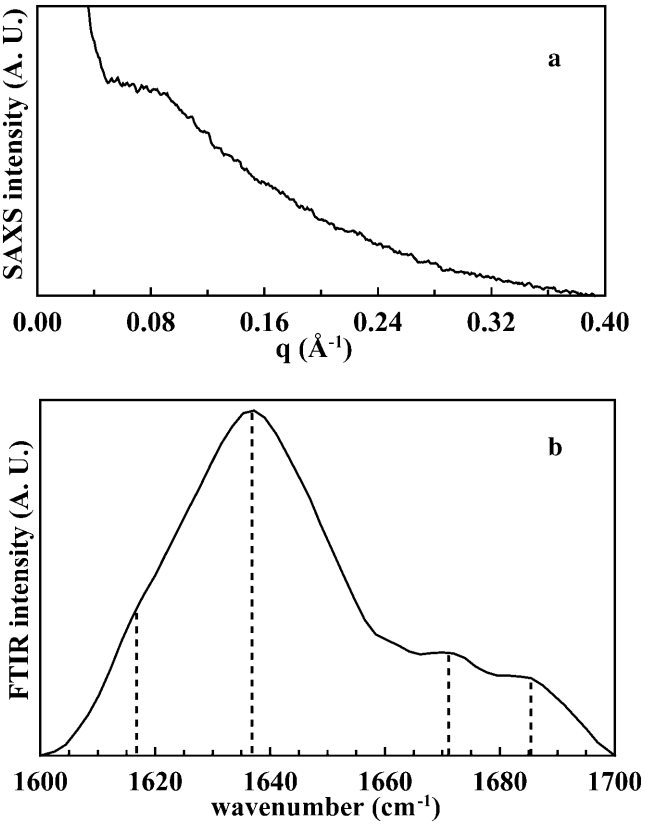

FIGURE 3 SAXS patterns (*a*) and FTIR spectrum after water signal and baseline corrections (*b*) obtained for a sample containing 2% (w/w) Lanreotide acetate. Both measurements were performed at 20°C.

peptide adopts a well-defined conformation, which exhibits the characteristics of a β-hairpin conformation (Table 1). Moreover, the presence of the antiparallel β-sheet network further supports the proposed presence of aggregates.

Therefore, part of the Lanreotide molecules self-associate below the 2.8% (w/w) macroscopic limit into β-sheet-based soluble aggregates, which may be the precursors of the structures formed above 2.8% (w/w) of Lanreotide acetate in water.

Lanreotide behavior at intermediate concentrations (3% ≤ [Lanreotide acetate] ≤ 20% w/w in water) and room temperature

From 3% to 20% (w/w) of Lanreotide acetate in water, the mixtures exhibit birefringence under crossed polarizers. Textures similar to developable surfaces (Bouligand, 1980; Kleman, 1980) were observed for Lanreotide acetate concentrations between 5% and 10% (w/w) (Fig. 4). These observations demonstrate the liquid crystalline organization of the nanotubes, in which the individual nanotubes can curve although remaining parallel one to another (Bouligand, 1980). This developable surfaces can be explained either by the curvature of long and rather flexible nanotubes or by

TABLE 1 Vibrational assignments of the IR bands of the amide I mode and relative contribution in % and in number of carbonyl groups of each secondary structures characterized for Lanreotide at different concentrations

	Antiparallel β-sheet				Random		Turn	
[Lan-ac] (% w/w)	Peak 1 (1620 ± 2 cm^{-1}) % area	Peak 2 (1691 ± 3 cm^{-1}) % area	Total (peak 1 and peak 2) % area	Number of carbonyl groups	1640 ± 1 cm^{-1} % area	Number of carbonyl groups	1663 ± 2 cm^{-1} % area	Number of carbonyl groups
2	22.4	14.0	36.4	3	47.2	4	16.4	1
5	23.0	17.0	40.0	3	37.4	3	22.6	2
10	24.6	17.1	41.7	3	36.3	3	22.0	2
10*	70.1	15.0	85.1	7	14.9	1	–	–
15	25.8	17.2	43.0	3	39.5	3	17.5	2
25	25.9	15.6	41.5	3	41.2	4	17.2	1
35	25.7	10.3	36.0	3	46.3	3	17.6	2
45	29.4	12.1	41.5	3	39.1	3	19.5	2
50	30.0	11.7	41.7	3	38.0	3	20.3	2

The sample 10* has been treated by β-mercaptoethanol.

short nanotubes This also indicates that the nanotubes are relatively flexible.

For concentrations over 10% (w/w) of Lanreotide acetate, no texture could be obtained probably because of the increase in the viscosity of the mixture with increasing peptide concentration.

To get more details about the structure of the nanotubes, VSAXS (Fig. 5) and SAXS experiments (Fig. 6) were performed on the Lanreotide acetate-water mixtures at room temperature. Between 5% and 10% (w/w) of Lanreotide acetate in water, VSAXS patterns exhibit Bragg peaks (Fig. 5). These reflections can be indexed by a hexagonal lattice model that reveals the crystallization of the nanotubes in a hexagonal network. The corresponding hexagonal unit cell parameter was calculated for each peptide concentration (Fig. 5, *inset*). The resulting values range from 363 Å to 367 Å, in good agreement with the local hexagonal organization observed on the electron micrographs. For Lanreotide acetate concentrations over 10% (w/w), no Bragg reflection could be detected. The nanotubes could not crystallize properly, probably because of viscosity, despite the short-range order previously visualized on the micrographs.

All the SAXS patterns recorded for mixtures in the concentration range 3–15% (w/w) of Lanreotide acetate

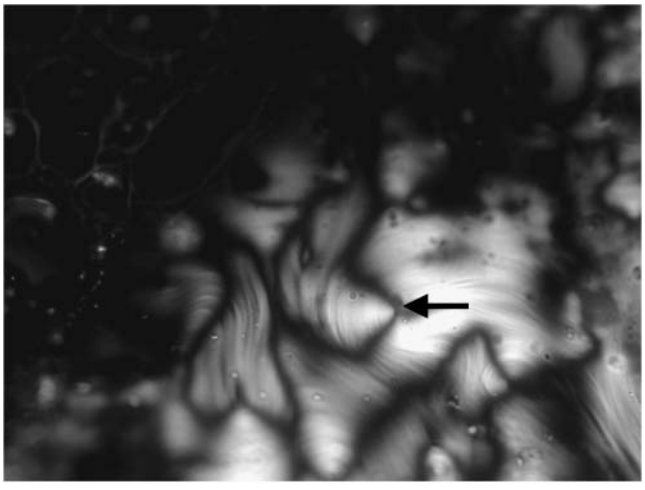

FIGURE 4 Developable surfaces obtained under polarized light with crossed polarizers at 20°C for a 7% (w/w) Lanreotide acetate in water mixture, conditioned in thin film between two glass slices. The arrow points out one of the highest points of curvatures of these specific textures.

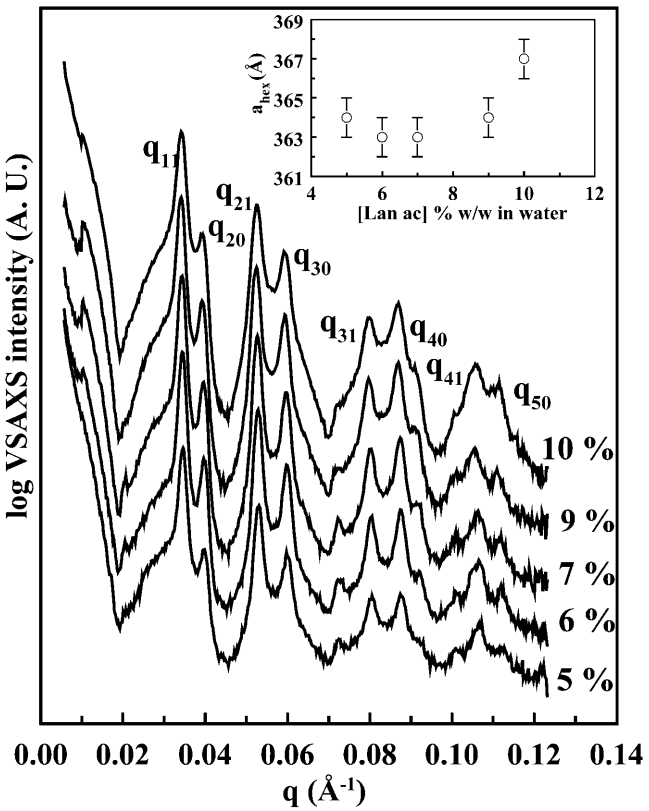

FIGURE 5 VSAXS patterns recorded at 20°C for different Lanreotide acetate in water mixtures as indicated on the traces. The Bragg peaks detected were indexed by a hexagonal lattice model (q_{kl} in figure). (*Inset*) Hexagonal unit parameter as a function of concentration.

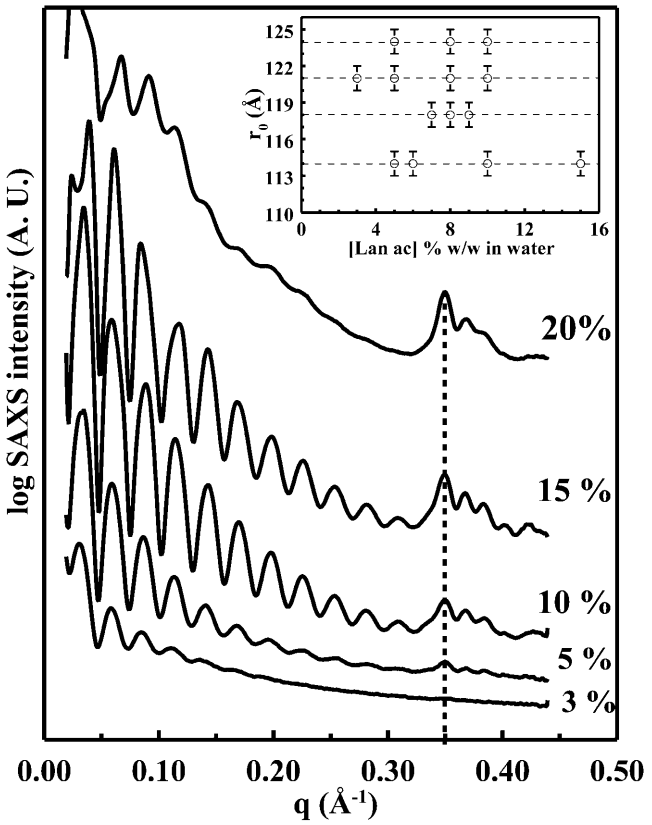

FIGURE 6 SAXS patterns recorded at 20°C for different Lanreotide acetate in water mixtures as indicated on the traces. The vertical dashed line points out the reflection at 0.35 $Å^{-1}$ visible on all the patterns. (*Inset*) Radii of the individual nanotubes calculated from the Bessel-like SAXS patterns as a function of Lanreotide acetate concentrations for different sets of experiments.

exhibit eleven oscillations, the last oscillation minimum being detected at ~0.30 $Å^{-1}$ (Fig. 6). These regular oscillations are well fitted by normalized Bessel functions of zero order $J_0^2(q.r_0)/q^2$. This mathematical model is the theoretical form factor of infinite hollow columns (Oster and Riley, 1952), where the only variable parameter is the mean radius of the column r_0. The product of this Bessel-like form factor with the Bragg reflections in the VSAXS pattern (see above) explains the experimental attenuation of the first order Bragg peak. The high number of Bessel oscillations demonstrates the monodispersity of the nanotubes radii within a same sample, in full agreement with the electron microscopy data. However, the radii calculated from the Bessel model are discrete from one sample to another, displaying the values of 114 Å, 118 Å, 121 Å, and 124 Å (Fig. 6, *inset*). This distribution of radii among the samples may depend upon nonidentified preparation parameters, such as thermal history or mixing strength. The Lanreotide nanotubes previously characterized for a 10% (w/w) mixture (Valéry et al., 2003) exhibit a radius of 121 Å. This study demonstrated that the walls of these nanotubes were made by the association of 26 filaments. According to this model, the different radii obtained correspond to nanotubes formed by a finite numbers of filaments going from 24 (114 Å) to 27 (127 Å) filaments.

The theoretic Bessel function is characterized by an infinite number of oscillations and corresponds to the model form factor of infinitely long and thin hollow columns. Therefore, the limited number of Bessel-like oscillations experimentally obtained for the Lanreotide nanotubes is due to the finite wall thickness of the hollow columns. An estimation of this wall thickness can be obtained by the reciprocal spacing of the last recorded oscillation minimum, which in all the cases is ~18 Å.

The SAXS patterns recorded for a 20% (w/w) Lanreotide acetate in water mixture exhibit a combination of the same oscillating features and of a central scattering (Fig. 6). At these concentrations, the nanotubes are still present but coexist with another scattering structure.

Finally, all the SAXS patterns recorded for Lanreotide acetate concentrations ranging from 3% to 20% (w/w) exhibit the same three reflections between 0.35 $Å^{-1}$ and 0.37 $Å^{-1}$ (Fig. 6). It was previously shown that these reflections, corresponding to repetitive distances between 17 Å and 18 Å, can be assigned to an antiparallel β-sheet network (Valéry et al., 2003).

FTIR and FT-Raman spectroscopies were used to determine the conformation of the Lanreotide backbone (Fig. 7 *a*) and of the disulfide bridge (Fig. 7 *c*), respectively. FTIR spectra were recorded at room temperature between 5% and

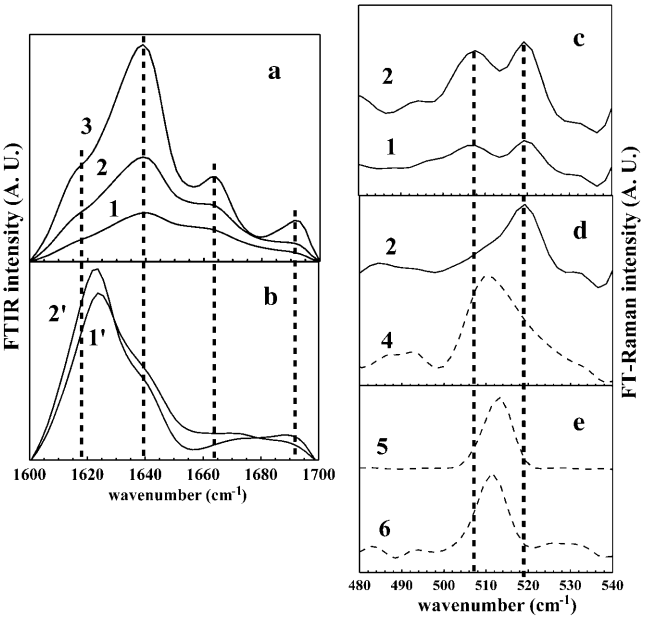

FIGURE 7 FTIR spectra in the frequencies of amide I vibrations (*a* and *b*) and FT-Raman spectra (*c–e*) measured at 20°C for 5% (*1*), 10% (*2*), and 15% (*3*) (w/w) Lanreotide acetate in water. The spectra 1′ and 2′ were obtained for Lanreotide concentration similar to the spectra 1 and 2, respectively, but in presence of β-mercaptoethanol (14 M). The spectrum (*4*) on *d* has been recorded for pure β-mercaptoethanol. The spectra 5 and 6 on *e* have been recorded for pure naphthalene and naphthalene in tetrahydrofurane, respectively.

20% (w/w) of Lanreotide acetate in water As previously done for the 2% sample, the analysis of these spectra was restricted to the region of the amide I vibrations (1600–1700 cm^{-1}). All of the spectra exhibit a similar well-defined shape composed of the four vibrations already detected for the 2% (w/w) sample. The recorded vibrations can be assigned to three conformations of hydrogen bonds in which the backbone carbonyls are involved: antiparallel β-sheet, turn, and random. The contribution of each of these vibrations to the normalized area of the total amide I band remains constant with the peptide concentration (Table 1). The conformation of the Lanreotide molecules within the nanotubes walls is thus well defined and independent on peptide concentration. Given the presence of eight backbone carbonyls in the Lanreotide sequence, these contributions allowed estimating that from one to two carbonyls are involved in a turn (19%), three carbonyls in an antiparallel β-sheet (41%), and three carbonyls in random conformations (40%) (Table 1).

To further confirm the assignments of the Lanreotide carbonyls vibrations, we recorded the FTIR spectra of Lanreotide-water mixtures reduced by β-mercaptoethanol, i.e., under conditions for which the disulfide bridge is reduced to free thiols (Fig. 7 *b*). Moreover, FT-Raman spectra were also recorded in presence and absence of β-mercaptoethanol to test the reduction efficiency and to determine the conformation of the disulfide bridge (Fig. 7, *c* and *d*). When compared to the nonreduced mixtures, the FTIR spectra of the reduced samples display a main loss of the 1640 cm^{-1} and 1660 cm^{-1} vibration bands and a relative increase of the 1620–1625 cm^{-1} vibration band. These changes in the FTIR spectra of the peptide indicate that the hydrogen bonds in random (1640 cm^{-1}) and turn (1660 cm^{-1}) conformations disappear in favor to H-bonds in antiparallel β-sheet conformation. From the quantification of the spectra, we determined that seven carbonyls were involved in an antiparallel β-sheet (85%) and that only one carbonyl is in random conformations (15%) (Table 1). The spectra of Lanreotide in presence of β-mercaptoethanol therefore indicate that the peptide adopts a linear conformation. Interestingly, SAXS experiments on these reduced mixtures show that the nanotubular structure is completely lost (data not shown).

The analysis of the FT-Raman spectra was focused on the frequency range associated to disulfide bonds vibrations (Sugeta et al., 1973) for two mixtures made of 15% and 20% (w/w) Lanreotide acetate in water (Fig. 7 *c*). These spectra exhibit two main vibrations. The FT-Raman vibration recorded at 519 cm^{-1} was attributed to the naphthalene ring since it was not affected by the presence of the reduction agent (Fig. 7 *d*). Moreover, the FT-Raman spectra of naphthalene either in powder or solubilized in tetrahydrofurane showed maxima at 511 cm^{-1} and 515 cm^{-1}, respectively (Fig. 7 *e*). These slight differences between the vibration frequencies of the naphthalene ring can be generated by the interaction of the aromatics found in all the different levels of organization of the peptide in the nanotubes (Valéry et al., 2003). On the other hand, the vibration at 508 cm^{-1} can be attributed to the disulfide bond since it disappears when the peptide is hydrated in the presence of β-mercaptoethanol (Fig. 7 *d*). Therefore, the lost of the H-bound in turn conformation (Fig. 7 *b*) can be directly related to the lost of the disulfide bridge. Moreover, in agreement with the literature, the range of the FT-Raman vibration band allows attributing a *gauche–gauche–gauche* conformation to the disulfide bridge (Li et al., 1991; Thamann, 1998; Vohnik et al., 1998).

Lanreotide behavior at high concentrations ([Lanreotide acetate] > 20% w/w in water) at room temperature

Over 20% (w/w) Lanreotide acetate in water, homogeneous birefringence was observed up to 50% (w/w), the most concentrated mixture examined (data not shown). No specific texture was obtained.

SAXS patterns were recorded at room temperature for Lanreotide acetate concentrations in the range 25–50% (w/w) (Fig. 8). All the corresponding patterns exhibit central and broad scattering at ~0.1 $Å^{-1}$. This broad scattering that could not be fitted by a simple model is due to the high polydispersity of the embedded nanotubes already visualized on the electron micrographs obtained for Lanreotide sample in this concentration range (Fig. 1).

The position of the principal peak at ~0.1 $Å^{-1}$ shifts toward the high angle (small distance) when the peptide concentration is increase. This evolution can be interpreted as a decrease of the spacing between the nanotubes walls, which is detected as a one-dimensional phenomenon by x-ray scattering, i.e., lamellar stacking. This interpretation has been verified by a general swelling model:

$$\phi = e/d_{XR} \Leftrightarrow d_{XR} = e\phi, \tag{2}$$

in which ϕ is the volume fraction of the structures, e is the thickness of the structures, and d_{XR} is the repetitive distance, i.e., the sum of the thickness of the structures and of the water layer is experimentally measured at the maximum of the central scattering peak recorded on the x-ray patterns. In the inset of Fig. 8, the distance given by the scattering peak position (d_{XR}) has been plotted versus the inverse of Lanreotide acetate weight fraction (assimilated to $1/\phi$) (Fig. 8, *inset*). The slope of the resulting linear regression gives an estimate of 15.5 Å for the thickness (e) of the walls of the embedded nanotubes. This value is in the same order of magnitude as the wall thickness of the individual nanotubes, determined by SAXS under 20% (w/w) Lanreotide acetate, i.e., 18 Å.

All the SAXS patterns recorded over 20% (w/w) Lanreotide acetate in water exhibit the far reflections between 0.35 $Å^{-1}$ and 0.37 $Å^{-1}$ already detected for lower concentrations. Although only the first order reflection (0.35

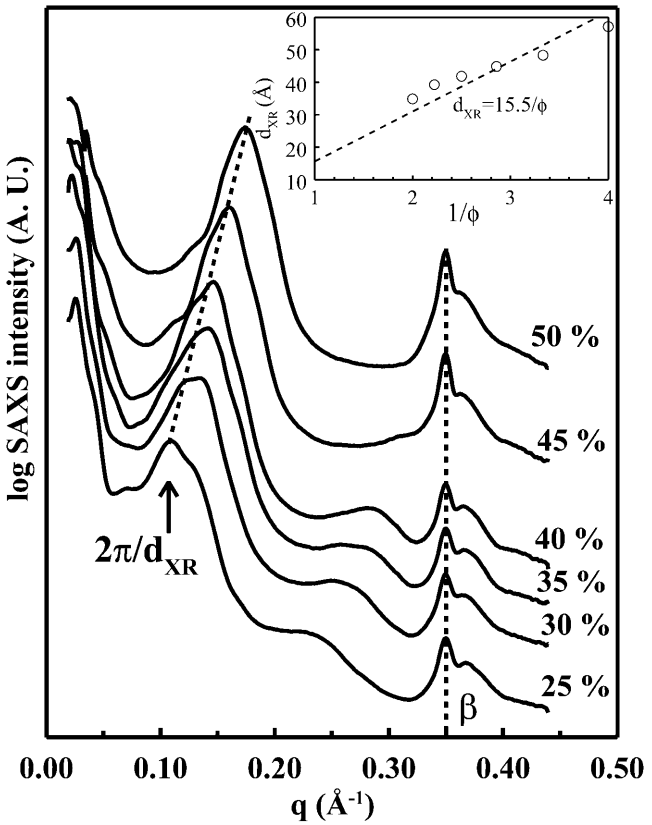

FIGURE 8 SAXS patterns recorded at 20°C for different Lanreotide acetate in water mixtures as indicated on the traces. The vertical dashed line underlines the conservation of the reflection at 0.35 Å^{-1}, whereas the other one underlines the evolution of the scattering broad peak with Lanreotide acetate concentration. (*Inset*) Evolution of distance deduced from the position of the maximum of the scattering broad peak with the inverse of the Lanreotide acetate weight fraction. The wall thickness *e* is deduced from the slope of the regression.

Å^{-1}) is correctly resolved, this result indicates that the antiparallel β-sheet organization of the peptide is conserved within the walls of the embedded nanotubes.

FTIR and FT-Raman spectra were recorded at room temperature from 25% to 50% (w/w) Lanreotide acetate in water (Fig. 9, *a* and *b*, respectively). The FTIR and FT-Raman vibrations positions and contributions are similar to those recorded for lower concentrations of peptide (Table 1) indicating that Lanreotide conformation remains unchanged.

All these results together demonstrate that the molecular and supramolecular organization adopted by Lanreotide in the embedded nanotubes are identical to the ones previously observed at lower concentration for individual nanotubes.

Thermotropism of the Lanreotide acetate-water mixtures

The effects of temperature on Lanreotide supramolecular structures were assessed by SAXS and VSAXS experiments. For SAXS experiments, the heating program was set from

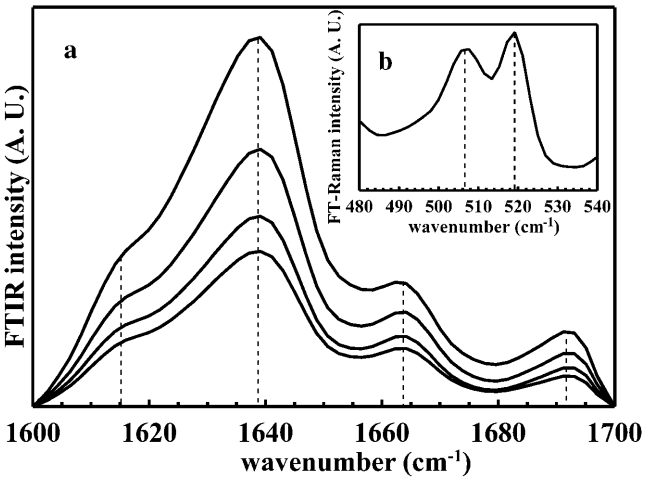

FIGURE 9 FTIR of amide I vibration bands (*a*) and Raman in the frequency range of the disulfide bond (*b*) spectra of Lanreotide acetate mixtures. (*a*) Lanreotide acetate concentrations (from the *bottom* to the *top*) of 25%, 35%, 45%, and 50% (w/w) in water. (*b*) Lanreotide acetate concentration 30% (w/w) in water. The dashed lines evidence the different maxima of each individual vibration bands.

14°C to 70°C at 0.5°C/min and the patterns were recorded every 2°C.

To illustrate the thermal behavior of the monodisperse individual nanotubes, the SAXS patterns of an 8% (w/w) Lanreotide acetate sample were plotted as a function of temperature (Fig. 10, *a* and *b*). From 20°C to 56°C, all the SAXS patterns exhibit the Bessel-like oscillating feature characteristic of the individual nanotubes (Fig. 10 *a*) combined with the three far reflections characteristic of the β-sheet network (Fig. 10 *b*). The reciprocal spacing of both signatures remain identical with the temperature increase, whereas their intensity progressively decreases until disappearance at 52°C. The Lanreotide nanotubes are progressively dissolved with temperature increase, whereas their structural parameters remain constant. Above 56°C, the SAXS patterns only exhibit a broad scattering peak (Fig. 10 *a*), which is similar to the one detected at room temperature below 2.8% (w/w) Lanreotide acetate in water (see Fig. 3). This similarity strongly suggests that heating induces the dissolution of the nanotubes into the corresponding β-sheet-based aggregates. This dissolution process has been detected from 3% to 20% (w/w), i.e., in the entire concentration domain of existence of monodisperse individual nanotubes at room temperature. The corresponding temperatures of dissolution were plotted as a function of peptide concentration, as well as the temperatures at which this scattering peak disappears, detected below 6% (w/w) (Fig. 10 *c*). A weak transition has been detected by DSC at high heating speed (10°C/min) in the temperature and concentration range of nanotubes dissolution. The corresponding enthalpy never exceeded 2 J/g (data not shown). A low energy is thus required for the dissolution of nanotubes into soluble aggregates.

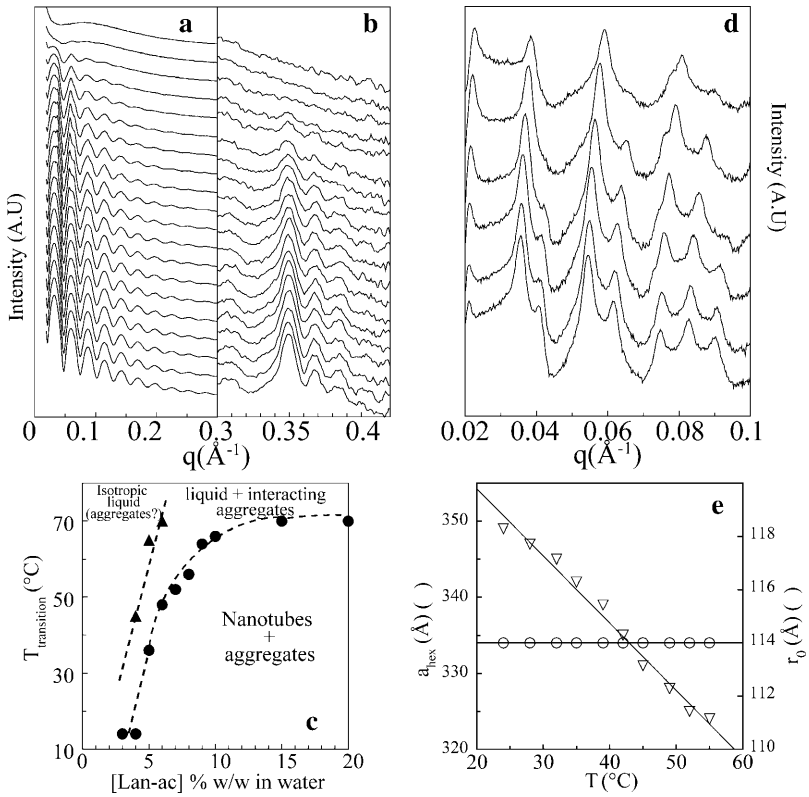

FIGURE 10 SAXS patterns (*a* and *b*) of an 8% w/w Lanreotide-water mixture during a heating program. (*a*) SAXS patterns focalized on the Bessel-like scattering oscillations. (*b*) SAXS patterns focalized on the scattering peaks at 0.35 Å. For both panels and from the bottom to the top, the traces have been recorded each 2°C, from 22°C to 60°C. (*c*) Evolution with the Lanreotide acetate weight fraction of the temperature of disappearance of the broad scattering peak at 0.1 Å^{-1} (▲) and of the Bessel-like pattern (●). (*d*) VSAXS patterns of 10% (w/w) Lanreotide acetate weight fraction during a cooling program. The patterns were recorded each 7°C from 56°C to 21°C from the top to the bottom. (*e*) Evolution of the hexagonal unit cell parameter (a_{hex}) and the column radius with temperature (data deduced from the patterns presented in *d*).

The reversibility of the dissolution of the individual nanotubes, i.e., their reconstitution, was obtained during a reverse cooling program of the heated samples. The SAXS data indicated that the nanotubes formed after this temperature cycle exhibit the same radii as the ones without thermal treatment (data not shown). However, the full recovery of the original patterns was only achieved after 24 h at room temperature, indicating a slow kinetic process of formation of the nanotubes.

For Lanreotide acetate concentrations ranging from 30% to 50% (w/w), the SAXS patterns recorded while heating up to 70°C remain identical to the ones obtained at room temperature. The temperature increase did not induce the dissolution of the embedded nanotubes into soluble precursors, indicating a better thermal stability of these complex structures compared to the individual nanotubes.

A 10% (w/w) Lanreotide acetate sample was examined by VSAXS as a function of temperature to assess the effects of varying the temperature on the hexagonal network, through the evolution of the corresponding Bragg reflections (Fig. 10 *d*). The measurements shown were performed during a decrease of temperature from 60°C to 20°C at 5°C/min. The decrease of temperature induces a shift of these reflections toward smaller distances (a higher reciprocal spacing q(Å^{-1})). The temperature decrease thus induces an increase of the hexagonal unit cell parameter, whereas the nanotubes radius remains unchanged (Fig. 10 *d*). The corresponding dilatation coefficient of the hexagonal network ($(da/dT) \times 1/a$) is negative, i.e., -3.10^{-3}°C^{-1}.

The phase diagram proposed in Fig. 11 summarizes the results obtained about the evolution of the structures formed by Lanreotide acetate in water with concentration and temperature. The experiments performed until 50% in Lanreotide acetate allowed the characterization of three different phases: 1), the isotropic liquid containing or not the soluble aggregates (Fig. 11, *blue dots*); 2), the pure individual nanotubes (Fig. 11, *red dots*), and 3), the pure embedded nanotubes (Fig. 11, *green dots*). The temperature and concentration domains of each of these phases were experimentally determined, and coexistence domains have been also delimited. To simplify the reading of the figure, drawings have been added on the bottom of the phase diagram to symbolize these different phases. The limit of existence of the soluble aggregates is indicated as a dashed line within the isotropic liquid domain.

Evolution of the water behavior with Lanreotide acetate concentration

Both water crystallization (Fig. 12 *a*) and melting of the frozen water (Fig. 12 *b*) in the Lanreotide mixtures, i.e., from 0% to 80% (w/w) of Lanreotide acetate in water, were examined by DSC (see Materials and Methods for details).

The crystallization experiments were performed from 20°C to −80°C since water molecules in confined spaces and/or adjacent to surfaces can be supercooled to very low temperatures (Grabielle-Madelmont and Perron, 1983; Hatakeyama and Hatakeyama, 1998; Cansell et al., 1991). From 2% to

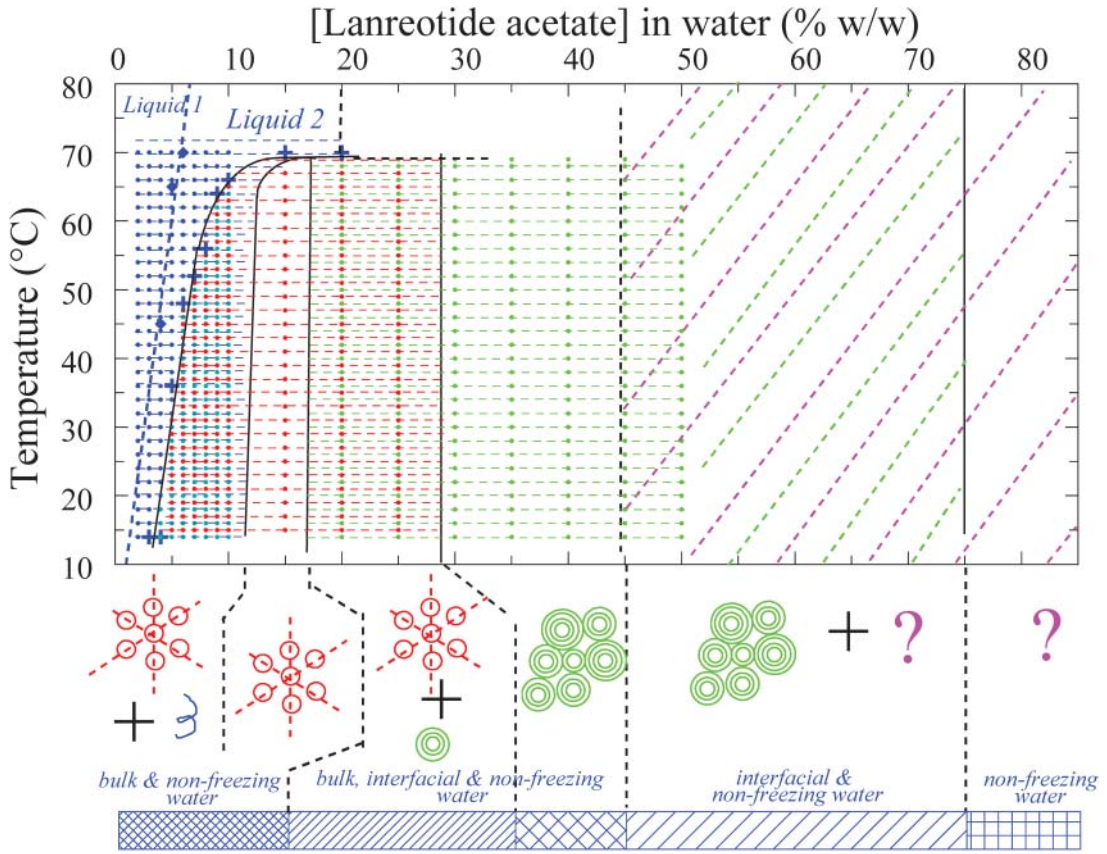

FIGURE 11 Phase diagram of Lanreotide acetate in water against temperature. The abscise is the concentration of Lanreotide acetate expressed in w/w % and the ordinate is the temperature in °C. The symbols used are blue dots, isotropic liquid; red dots, nanotubes; green dots, embedded nanotubes; and plus signs, limit between the liquid containing or not interacting aggregates. Superposition of the following symbols, blue dots and red dots, and red dots and green dots, indicates coexistence of isotropic liquid and nanotubes and nanotubes and embedded structures, respectively. The purple dashed lines on the diagram indicates that other phases for which we have no structural data are present either in coexistence with the embedded structures (*green dots* and *green dashed line*) or alone. Under the phase diagram, some simple schemes represent the different structures determined in this work and the colors are related to the colors used above: in blue we have drawn soluble filaments, in red a hexagonal lattice of nanotubes with monodisperse diameters, and in green polydisperse embedded nanotubes. On the bottom of the figure are indicated the different types of water regimes determined as a function of peptide concentration by DSC experiments on water crystallization and melting. See Fig. 13 for details.

50% (w/w) of Lanreotide acetate in water the crystallization curves exhibit a single exothermic peak at −20°C ± 5°C, i.e., similar to the crystallization temperature of pure water under the same experimental conditions (Fig. 12 *a*). For 60% (w/w) Lanreotide acetate in water, the crystallization curve is clearly shifted toward a lower temperature, and above 70% (w/w) the absence of thermal event indicates that the remaining water is not able to freeze, even at very low temperature. This nonfreezing water corresponds to water molecules involved in the immediate environment of the Lanreotide molecules. Such a behavior is a general phenomenon encountered in aqueous preparations involving macromolecules or extensive surfaces (Franks, 1982b).

The melting of the frozen water also depends on the Lanreotide concentration (Fig. 12 *b*), and four different behaviors can be characterized: 1), up to 10%, the melting of the frozen water occurs at 0°C as expected for bulk water; 2), from 15% to 40%, part of the frozen water melts at a temperature below 0°C, i.e., −8°C ± 1°C (Figs. 12 *b*, *arrows*, and 13 *a*, *solid triangles*), the other part melting at 0°C as bulk water. This behavior indicates two types of water. At the interface between bulk water and the nonfreezing water molecules in the immediate vicinity of the Lanreotide acetate molecules exist some water molecules that are influenced by their environment leading to the melting point depression. This type of water is designed as interfacial water. 3), From 40% to 60%, all the frozen water melts below 0°C and the T_{on} decreases with the increase of Lanreotide concentration (Figs. 12 *b* and 13 *a*); 4), at 75%, no thermal event can be detected all over the temperature range examined, in agreement with the absence of crystallization observed during the cooling scans and evidences the presence of nonfreezing water (Figs. 12 *b* and 13 *a*).

To understand the water behavior as a function of peptide concentration, the melting curves have been analyzed to estimate the water/peptide weight ratio for each kind of water evidenced from both the water crystallization and the melting of frozen water curves, i.e., the bulk (melting at 0°C), the

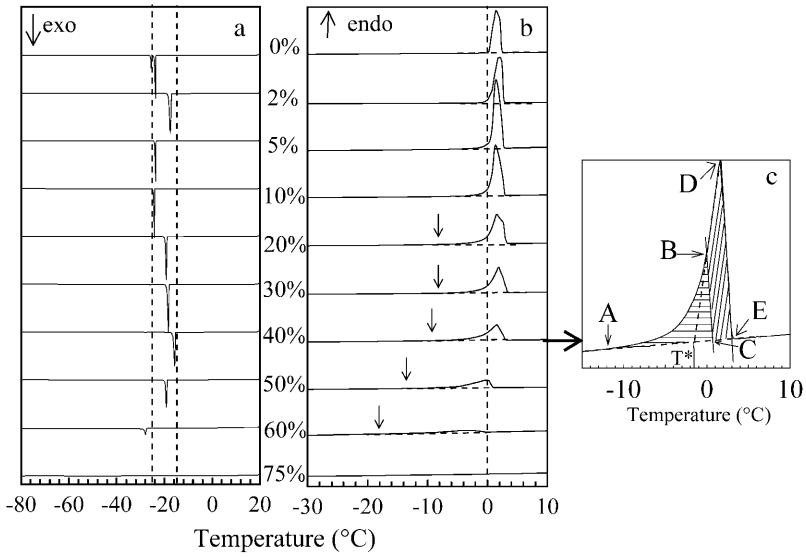

FIGURE 12 (*a*) Crystallization curves of water as a function of Lanreotide acetate concentration (% w/w in water). The mixtures were analyzed at a cooling rate of 5°C/min in the temperature range from 20°C to −80°C. The dashed lines indicate the temperature range of the water crystallization. (*b*) Melting curves of frozen water as a function of Lanreotide acetate concentration (% w/w in water). The mixtures were analyzed at a heating rate of 2°C/min in the temperature range from −80°C to 20°C. The dashed line indicates the melting temperature of bulk water, i.e., 0°C. The arrows indicate the T_{on} of the frozen water melting below 0°C. (*c*) Description of the procedure for the interpretation of the curves exhibiting both bulk and interfacial frozen water melting (see Materials and Methods section).

interfacial (melting below 0°C), and nonfreezing waters. For this purpose the melting enthalpy change of the interfacial and bulk water have been estimated according to the procedure described in Materials and Methods (Fig. 13 *c*). These enthalpy changes normalized to the enthalpy change of bulk water, i.e., 333 J/g, allowed to calculate for each mixture the H_20_{interf}/peptide (Fig. 13 *b*, *open triangles*) and H_20_{bulk}/peptide ratio (Fig. 13 *b*, *open circles*) that have been expressed in w/w.

To access the $H_20_{nonfreezing}$/peptide ratio, we calculated the sum of the melting enthalpy changes of the bulk (Fig. 13 *c*, *open circles*) and interfacial water (Fig. 13 *c*, *open diamonds*) that results in the curve plotted in Fig. 13 *c* (*open squares*). This last curve represents the enthalpy change of the melting of the total freezable water in the sample. When compared with the theoretical evolution of the enthalpy of melting of the whole water content in the mixtures (Fig. 13 *c*, *dashed line*), the experimental curve shows that, in addition of the two types of water characterized above, part of the water present in the sample is unable to freeze and subsequently to melt (Grabielle-Madelmont and Perron, 1983). The experimentally observed dependence of the melting enthalpy versus fraction Lanreotide can be described by two straight lines the intercept of which occurring at ~42% (w/w) of Lanreotide acetate in water. The comparison of the experimental curve to the theoretical one leads to estimating the $H_20_{nonfreezing}$/peptide (w/w) for each Lan-ac wt % in the mixture (Fig. 13 *b*, *open squares*). From the evolution $H_20_{nonfreezing}$/peptide (w/w) with the peptide concentration, we can notice that until 42% in peptide this ratio remains constant at 0.6 g/g Lanreotide acetate, and then continuously decreases for higher peptide concentrations.

From the water behavior we could determine five different concentration domains that are related to the supramolecular structures formed by the peptide in solution. These five domains have been indicated in Fig. 11 (*bottom*) in relation with the existence domain of the phases identified by the structural data.

From 0% to15%, all the frozen water melts at 0°C. In this peptide concentration range, the H_20_{bulk}/peptide (w/w) decreases whereas the $H_20_{nonfreezing}$/peptide remains constant at ~0.6 g water/g peptide. From the structural studies described above we know that in this range of concentration, from 3% to 15%, monodispersed nanotubes are formed. Moreover, considering the aggregates already characterized at low peptide concentration, i.e., below 2.8%, this result indicating that the hydration mode of the aggregates is identical to the hydration mode of the nanotubes, supports the idea that the aggregates present at low concentration are the precursors of the hollow columns and structurally closed to them.

From 15% to 35%, compared to the lower concentration domain described, an additional kind of water appears, i.e., the interfacial water melting below 0°C. In this concentration range, H_20_{bulk}/peptide decreases, the $H_20_{nonfreezing}$/peptide still remains constant, and the H_20_{interf}/peptide increases from 0.4 g/g to 0.6 g/g of peptide. In this concentration domain, embedded nanotubes are formed. The water in between the walls of two nanotubes embedded in one into the other can easily explain the appearance of the interfacial water.

From 35% to 42%, the $H_20_{nonfreezing}$/peptide is still constant whereas the H_20_{interf}/peptide starts to decrease with the peptide concentration. Until 42%, we still have visualized embedded nanotubes. Then, this concentration domain may correspond to a pure embedded nanotubes phase.

From 42% to 75%, bulk water no longer exists in the sample since all the water able to freeze entirely melts below 0°C with temperatures significantly decreasing

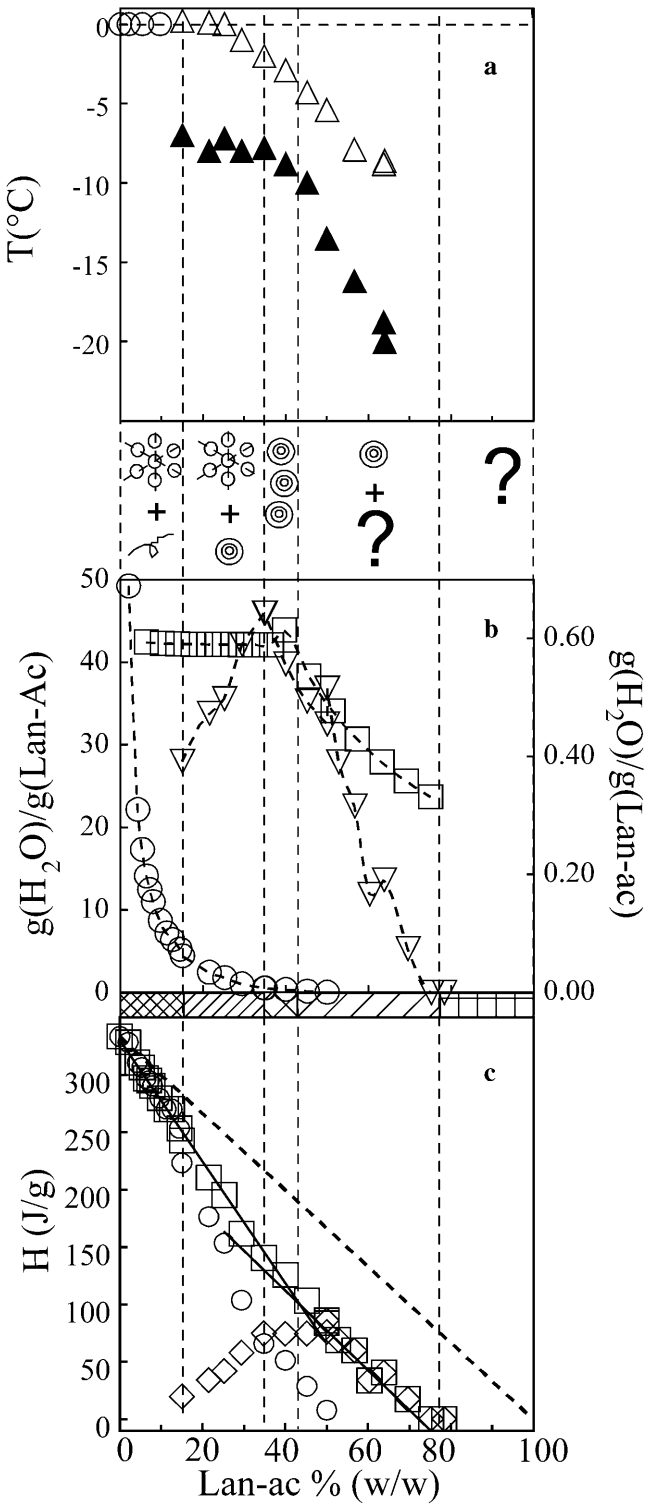

FIGURE 13 (*a*) Evolution of the T_{on} of melting of the bulk water (-○-) and of the interfacial water (*point A* in Fig. 12 *c*) (-▲-) with Lan-ac weight fraction (%). The (-△-) represents T^* (Fig. 12 *c*), the average temperature of the water melting below 0°C (see Materials and Methods for details). (*b*) Evolution with Lan-ac weight fraction (%) of the H_2O_{bulk}/Lan-ac (-○-, *left scale*), the H_2O_{interf}/Lan-ac (-∇-, *right scale*) ,and the $H_2O_{nonfreezing}$/Lan-ac (-□-, *right scale*) weight ratio. (*c*) Enthalpy change of melting of the bulk water (○), of the interfacial (◇), and of the total freezable water (□), i.e., the sum of the enthalpies if both bulk and interfacial waters. The dashed line represents the theoretical enthalpy change associated to the water melting assuming that all the water present in the sample behave as bulk water. In between *a* and *b*, the small drawings already used in Fig. 11 to schematize the structures formed by Lanreotide has been also used to delimit their existence domains as visualized by the thermal behavior of water. Moreover the ''?'' indicates that from the DSC data evidences have been obtained for the existence of a new phase, for which we however have no structural information. In between *b* and *c*, we have used the schemes used in Fig. 11 to indicate the different regimes of water behavior.

from −15°C to −20°C as a result of the growing impact of the Lanreotide acetate organization on the thermal behavior of the interfacial water (Fig. 12 *b*). Moreover, both the $H_20_{nonfreezing}$/peptide and H_20_{intef}/peptide continuously decrease with the increasing of the peptide concentration, and, at 75%, the H_20_{interf} has totally disappeared (Fig. 13 *b*). It is notable that the onset temperature of the DSC peak gradually decreases from −2°C to −10°C (Fig. 13 *a*, *open triangles*), whereas the very beginning of the transition is clearly shifted toward much lower temperatures from −8°C to −20°C (Figs. 12 *b*, *arrows*, and 13 *a*, *solid triangles*). This means that a fraction of the interfacial water is more and more influenced by its environment. For this concentration domain, we proposed that embedded nanotubes coexist with another structure that we have not characterized (Fig. 11, *purple dashed lines* and ''?'').

For concentration higher than 75%, the water in the samples neither crystallizes nor melts, giving no further information.

DISCUSSION

Lanreotide acetate/water mixtures were systematically studied as a function of peptide concentration and temperature using complementary techniques such as electron and optical microscopies, VSAXS, SAXS, FTIR, and FT-Raman. From these data the phase diagram of Lanreotide acetate in water is proposed (Fig. 11) in which three different phases have been characterized in the Lanreotide-water system, i.e., the liquid, the individual nanotubes, and the embedded nanotubes phases. In parallel, we also characterized the thermal behavior of the water in the mixtures and showed that the presence of the peptide in solution induces three different behaviors for the water that appears or disappears depending on the phase present in solution.

The individual nanotubes domain

Between 3% and 20% (w/w) Lanreotide acetate in water at room temperature, remarkably uniform individual nanotubes in a hexagonal lattice (unit parameter of 365 Å), are observed.

Indeed the positional long-range order observed by SAXS and the developable surfaces demonstrate that the nanotubes

are packed in a 2D hexagonal crystal. The reduction of the longitudinal length could explain the developable surface but would not be compatible with the hexagonal packing of the columns. Indeed, Albouy et al. (1995) have demonstrated with diamide molecules that the reduction of the column length produces a transition from a columnar hexagonal lattice to a Nematic columnar lattice. Therefore, the only possibility of observing a columnar order is that columns or nanotubes are very long compared to their diameter (Artzner et al., 1997). The core size of disclinaison give a good approximation of the flexibility of the columns. In the case of Lanreotide nanotubes, this core size is smaller than 1 μm and indicates that the nanotubes are relatively flexible.

These objects display a monodisperse radius within the same sample but display discrete radii values from one sample to another, in the range 114–124 Å, without any dependence on concentration. According to previous structural works on Lanreotide monodisperse nanotubes (Valéry et al., 2003), these values are related to a varying number of associated filaments per nanotubes, from 24 to 27, respectively. If the different radii obtained are not related to the concentration, they must be related to not yet controlled parameters, as for example the force used during the water and peptide mixing. On the contrary, among all the mixtures tested, a constant thickness of 18 Å was estimated for the walls of the nanotubes.

The disappearance of the columnar phase observed upon increasing the temperature allowed to determine the limits of existence of this phase. Interestingly the radius of the nanotubes is not affected by temperature increase. This result indicates that this domain is biphasic, i.e., coexistence between isotropic liquid and columnar phase. However, the hexagonal packing parameter decreases with temperature increase, with a dilatation coefficient of -3.10^{-3} Å/°C. This negative value can be interpreted as a decrease of electrostatic repulsion between the highly positively charged surfaces of the nanotubes, with temperature increase (Valéry et al., 2003).

The thermal behavior of the individual nanotubes evidenced a dissolution process of these structures into the soluble aggregates detected at room temperature under 2.8% (w/w) of Lanreotide acetate in water (limit of existence of the columnar phase). Therefore, the individual nanotubes coexist with the soluble aggregates, and the concentration of these aggregates depends on temperature.

The embedded nanotubes domain

The embedded nanotubes are detected at room temperature from 20% to 50% (w/w) of Lanreotide acetate in water. The supramolecular structures in this phase were characterized by electron microscopy and SAXS.

The electron micrographs obtained from the longitudinal cut of the object could have been obtained either by the coiling up of a flexible sheet or by individual nanotubes embedded in each other's. However, these two possible arrangements would have given very different imprint for the transversal cut: the former would have given the image of a unique wall coiled up on itself, whereas the latter would have given the image of individual circles of different diameters. Indeed, the electron microscopy pictures of the transversal cuts show this last organization and demonstrate the embodiment of the nanotubes.

The structural data show that the wall thickness of the embedded nanotubes (~15.5 Å), the conformation of the peptide, and the intermolecular interactions involved (β-sheet networks) remain identical to those found for the individual nanotubes. The electron micrographs also show that the embedded structures are formed by the embodiment of smaller or larger nanotubes compared to the ones formed below 20% in peptide. This observation suggests that nanotubes are inside or outside the individual ones. Furthermore, temperature-dependant SAXS experiments showed a higher thermal stability for these embedded structures than for the individual nanotubes.

Water behavior corresponding to the different structures

The study of water crystallization and melting in the Lanreotide acetate samples showed the existence of three different water states: bulk water, interfacial water, and nonfreezing water. These water states were characterized alone or in coexistence, upon Lanreotide acetate concentration, and are related to the different supramolecular organizations of Lanreotide.

Considering the interfacial water characterized by a melting below 0°C, it appears at a peptide concentration above 15% and is detectable until 75% Lanreotide actetate in water. More precisely, the interfacial water/peptide weight ratio increases from 15% to 35% and decrease until it disappears at 70–75% peptide. This appearance of the interfacial water is likely related to the appearance of the embedded columns into the samples. Indeed, the staking of the nanotube walls into the embedded nanotubes would modify the properties of the water entrapped in between these walls. Interestingly, between 15% and 35% Lan-ac weight fraction, the nonfreezing water/peptide weight ratio is constant, i.e., 0.6 g/g Lan-ac. This concentration domain likely represents the domain in which the concentration of embedded nanotubes is increasing.

At ~42% in Lanc-ac, the bulk water disappears and the nonfreezing water/peptide weight ratio starts to decrease. This decrease together with both the interfacial water/peptide weight ratio decrease and the absence of bulk water strongly suggest that some new organization or aggregates are formed in these samples in coexistence with embedded nanotubes.

At 75% Lan-ac weight fraction, no more water is able neither to freeze nor to melt, indicating that for higher concentration the embedded nanotube structures are not formed anymore.

If we consider the nonfreezing water/peptide weight ratio of 0.6 determined from 0% to 42% in peptide, this value correspond to ~40 molecules of water per molecule of peptide that are not able to melt nor to freeze. In the range from 0% to 42% and considering the molecular volume of water V (~30 Å^3), the surface occupied by one molecule of peptide in the wall of a nanotube S (190 Å^2) (Valéry et al., 2003), we can write

$$N \times V = S \times e, \tag{3}$$

where N is the number of water molecule in interaction with one peptide in the structure ($N = 36$), and e is the water layer around one molecule of peptide. The water layer has then been determined at ~5.7 Å. Considering the hollow nanotubes and the fact that the wall of a hollow tube is composed of a double layer of peptide molecules, the total layer of water would be around 11.4 Å, which is in the order of magnitude of the nanotube wall thickness. From the XR data, the interdistance determined from the swelling law gives a value of 37 Å for a 42% Lan-ac sample.

Considering that for this sample we have no more bulk water, all the water would be found in between the walls of the nanotubes. Then we can write

$$d_{\mathrm{XR}} = e_{\mathrm{tube}} + e_{\mathrm{nonfreezing\ water}} + e_{\mathrm{interfacial\ water}}, \tag{4}$$

where d_{XR} is the interdistance measured by the SAXS experiments, i.e., 37 Å, e_{tube} is the wall thickness of the individual embedded nanotubes, i.e., 15.5 Å, and $e_{\mathrm{nonfreezing\ water}}$ is the thickness of the nonfreezing water layer, i.e., 11.4 Å. From this equation we can then deduce that the thickness of the interfacial water layer, i.e., $e_{\mathrm{interfacial\ water}}$, would be ~10.1 Å, which is in the same order of magnitude of the thickness of the nonfreezing water layer (11.4 Å). This is in agreement with the DSC data that showed that the nonfreezing water/peptide and the interfacial water/peptide ratios in this concentration range are in the same order of magnitude, i.e., ~0.6 g H_2O/g peptide. Therefore, this interfacial water that only appears when the nanotubes start to grow concentrically is essentially located in between the walls of the resulting embedded nanotubes and can be characterized as enclosed water. Moreover the maximal quantity of enclosed water is reached for an interdistance of 37 Å between the walls of the nanotubes.

A mechanism for nanotube formation

A mechanism for nanotubes formation is proposed from the properties and domains of existence of the different Lanreotide supramolecular organizations detected, i.e., soluble aggregates, individual monodisperse nanotubes, and embedded nanotubes. At low Lanreotide acetate concentration (below 2.8% w/w) and room temperature, soluble aggregates are formed. We have no direct structural information on these aggregates. However, we propose these to be the filaments associated in the walls of the nanotubes. The evidences in favor of the formation of filaments in solution are 1), the size of the aggregates is below 20 Å; 2), their hydration mode is the same as the one of the individual nanotubes; 3), the β-sheet networks are already present in the structure of the aggregates; 4), the temperature dependent and reversible dissolution process of the individual nanotubes into the same soluble aggregates as the ones characterized at low peptide concentration; and 5), the low enthalpy associated with this dissolution process. Such a preaggregation process has also been proposed by Walsh et al. (1999) before the formation of fibrils of amyloid β-protein, and these authors could show that the protofibrils were in dynamic equilibrium with the fibrils. The very low peptide concentration domain has not been explored, and therefore no direct information about the mechanism by which these filaments would be formed is available yet. However, we can hypothesize that the first aggregate to be formed would be an antiparallel dimer of the peptide that is the smallest repetitive structural unit in the organization the nanotube wall (Valéry et al., 2003). The important characteristic of these antiparallel dimers would be the interaction between the aromatic via the D-Naph and the Phe residues and the partitioning of the charge of the peptide. The net charge of the peptide is +2 (the lysine residue and the N-terminal). The conformation of the peptide in the proposed dimer positions these positively charged residues on the two branches of the β-hairpin, i.e., at the two extremes of the dimer as far as possible from each other. We therefore postulate that, in addition to the hydrophobic effect, the minimization of the electrostatic repulsion will be the other driving force for the formation of this antiparallel dimer. The stacking of these antiparallel dimers by the formation of the β-sheet network will lead to the formation of the filaments. Sunde and Blake (1997) and Serpell et al. (1999) have also underlined the importance of aromatic residues and have proposed for the growth of β-amyloid fibers that the stacking of aromatics is the very first nucleation process. In our case, the additional electrostatic repulsion will further promote the formation of these highly ordered structures.

When the critical peptide concentration of 3% is reached, 24–27 of these filaments self-associate into hollow columns. Interestingly, the facts that 1), the diameter of the columns is monodisperse and 2), at 5% in Lanreotide acetate the columns are already organized in a hexagonal lattice suggest that, when the first column is formed, the next one is formed just near it and that the hexagonal lattice would act at a template and fix the size of these structures. When the concentration of hollow columns would be maximal, i.e., all the sample volume is occupied by the hexagonal packing of the hollow columns, a further increase in peptide concentration would cause the formation of new nanotubes from the

filaments dissolved in the water either inside or outside the nanotubes leading to the embedded structures observed at high peptide concentrations. Such a hierarchical mechanism of fiber formation has already proposed by Aggeli et al. (2001), for a rod-shaped chiral oligopeptide, where the final fibers is produced by the progressive stacking of an initial long twisted ribbon. Interestingly, these authors observed that the ribbon twisting decreases with the number of self-associated ribbons. In our case, for the embedded columns, the radii of the individual column change also.

Importance of the peptide conformation on the supramolecular arrangement

The molecular and supramolecular organization of the peptide in all the mesophases characterized in this work remains constant. All the data promote the peptide self-association mode determined by Valéry et al. (2003) on single nanotubes at 10% w/w Lanreotide acetate in water. In particular, these authors showed that the β-hairpin conformation of the peptide was constrained by a disulfide bond lying in a plane orthogonal to the backbone. A network of hydrogen bonds in an antiparallel β-sheet symmetry then forms the walls of the nanotubes. To characterize the importance of the disulfide bridge in the self-association mode of Lanreotide, we have treated different peptide-water mixtures by β-mercaptoethanol and saw that the disappearance of the disulfide bridge induces the disruption of both the β-hairpin conformation of the peptide and the nanotube organization. This observations show that besides achieving the segregation of the aromatic residues within the peptide itself, the presence of the disulfide bridge is crucial for the formation of the nanotubular structures. El-Agnaf et al. (2001) have shown for the amyloid peptide ABri that the reduction of the disulfide bond present in the peptide inhibits the formation of fibrils. Moreover, they showed by molecular modeling that the disulfide bridge stabilizes a three-stranded pleated sheet with the hydrophobic residues predominantly localized on one of its faces, a conformation that shares some characteristics with the one proposed for the Lanreotide acetate.

We conclude that the peculiar symmetries and interactions involved in the Lanreotide self-organization can be compared with the characteristics of the amyloid β-peptide fibers. Both organizations rely on an antiparallel β-sheet organization of a β-hairpin peptide into hierarchical assemblies and on the importance of highly hydrophobic residues for the nucleation process (Sunde and Blake, 1997; Serpell et al., 1999). Therefore, Lanreotide emerges as an interesting model peptide to investigate general protein-like molecular self-assembly processes leading to well-organized fibers and nanotubes. This very small peptide contains all the information necessary to form these incredibly large structures and allows, by relatively simple chemical substitutions, testing the role played by each residue in this hierarchical self-assembling process.

CONCLUSION

Considering the pharmaceutical application of the Lanreotide-water gels, the dissolution process of the columnar liquid crystals is of major interest. The thermodynamic stability of the nanotubes and the dynamic equilibrium between the nanotubes and precursors in solution support the idea that dissolution would proceed by perturbation of this equilibrium. Although this study does not allow accessing the physiological parameter that would perturb the Lanreotide organization, the phase diagram depicted here shows that the embedded columns are thermodynamically much more stable than the hollow ones. Interestingly, the Autogel that exhibits the sustained and controlled release properties when used as subcutaneous implant is formed at 30% in water, i.e., in the form of embedded columns.

The Lanreotide-water phase diagram was successfully elucidated on both the supramolecular and molecular scale. The tubular self-assemblies of Lanreotide were characterized as thermodynamically stable over a wide range of concentration and temperature. No temperature effect was detected on the structural parameters of these assemblies. The self-assembly architecture was identical for all the structures determined, i.e., antiparallel β-sheet networks and aromatic stacking of the peptide molecules that remain in a β-hairpin conformation (Valéry et al., 2003). As a mechanism, we propose that soluble filaments would form at low peptide concentration and the filaments self-associate to form hollow columns when a critical concentration is reached. The embedded columns then appear, when the total hollow columns concentration reaches its maximum. These structures would be induced by the formation of larger and smaller hollow columns from the filaments present either outside or inside the previously formed hollow columns.

Lanreotide self-assemblies are remarkably stable organizations, which already showed their exceptional properties as peptide-based biomaterials in the pharmaceutical domain (Cherif-Cheikh et al., 1998). The understanding of Lanreotide self-assembly process is promising for the development of future functional biomaterials, for which the current development of supramolecular chemistry (Lehn, 2002) provides a wide set of applications. This system may also be useful to characterize the properties of different water states and in particular to study the enclosed water that has been observed in between the walls of the concentric nanotubes. Moreover, this peptide can be studied as a model for amyloid fibril growth, a system with which Lanreotide already shares important properties all the way from the molecular conformation to the self-assembling process. In particular, the study of derivatives of Lanreotide would provide interesting information about the relevant interactions implicated in Lanreotide liquid crystalline growth. Furthermore, the study of the very first steps of Lanreotide self-association (very low concentration domain) would give crucial information about

the basic molecular interactions at the origin of the fiber growth.

We are grateful to Pilar Calvo who first observed the liquid crystals formed by Lanreotide-water mixtures and to T. Narayanan and D. Durand for their help and advice regarding the experiments performed on the high brilliance ID2A at European Synchrotron Radiation Facility (Grenoble, France) and D43 at Laboratoire pour l'Utilisation du Rayonnement Electromagnétique (Orsay, France) synchrotron beam lines. European Synchrotron Radiation Facility is acknowledged for provision of beam time (SC801).

This work was supported by Centre National de la Recherche Scientifique (AC Nanosciences/Nanotechnologies), by the Université Paris-Sud, and by Ipsen Pharma/Centre National de la Recherche Scientifique CIFRE grant (Céline Valéry).

REFERENCES

Aggeli, A., I. A. Nyrkova, M. Bell, R. Harding, L. Carrick, T. C. B. McLeish, A. N. Semenov, and N. Boden. 2001. Hierarchical self-assembly of chiral rod-like molecules as a model for peptide β-sheet tapes, ribbons, fibrils, and fibers. *Proc. Natl. Acad. Sci. USA.* 98:11857–11862.

Albouy, P. A., D. Guillon, B. Heinrich, A.-M. Levelut, and J. Malthête. 1995. Structural study of the nematic and hexagonal columnar phases of wire shaped self assemblies of thermotropic mesogens. *J. Phys. II (Paris).* 5:1617–1634.

Archibald, D. D., and P. Yager. 1992. Microstructural polymorphism in bovine brain galactocerebroside and its two major subfractions. *Biochemistry.* 31:9045–9055.

Artzner, F., M. Veber, M. Clerc, and A. M. Levelut. 1997. Evidence of the nematic, hexagonal and rectangular columnar phases of thermotropic ionic liquid crystals by SAXS. *Liq. Cryst.* 23:27–33.

Banakar, U. V. 1997. Advances and opportunities in delivery of therapeutic proteins and peptides. *J. Biomater. Appl.* 11:377–429.

Bandekar, J. 1992. Amide modes and protein conformation. *Biochim. Biophys. Acta.* 1120:123–143.

Bong, D. T., T. D. Clark, J. R. Granja, and M. R. Ghadiri. 2001. Self-assembling organic nanotubes. *Angew. Chem. Int. Ed. Engl.* 40:988–1011.

Bouligand, Y. 1980. Defects and textures of hexagonal discotics. *J. Phys.-Paris.* 41:1307–1315.

Byler, M., and H. Susi. 1986. Examination of the secondary structure of proteins by deconvolved FTIR spectra. *Biopolymers.* 25:469–487.

Cansell, F., C. Grabielle-Madelmont, and M. Ollivon. 1991. Characterization of the aqueous phase and the water-polymer interface in latex suspensions by differential scanning calorimetry. *J. Colloid Interface Sci.* 144:1–17.

Cherif-Cheikh, R., F. Bismuth, M. L. Torres, R. Alloza, M. T. Bosch, M. Montes, E. Fuster, J. Valles, J. A. Cordero, C. Peraire, R. Obach, and R. M. Antonijoan. 1998. Autogel registered trade mark: a new lanreotide prolonged release formulation. *Proceed. Intern. Symp. Control. Rel. Bioact. Mater.* 25:798–799.

El-Agnaf, O. M. A., J. M. Sheridan, C. Sidera, G. Siligardi, R. Hussain, P. I. Haris, and B. M. Austen. 2001. Effect of disulfide bridge and the C-terminal extension on the oligomerization of the amyloid peptide ABri implicated in familial British dementia. *Biochemistry.* 40:3449–3457.

Franks, F. 1982a. The properties of aqueous solutions at subzero temperature. *In* Water: A Comprehensive Treatise, Vol. 7. Felix Franks, editor. Plenum Press, New York and London. 315–338.

Franks, F. 1982b. The dynamics of water in heterogeneous systems. *In* Water: A Comprehensive Treatise, Vol. 7. Felix Franks, editor. Plenum Press, New York and London. 339–393.

Gazit, E. 2002. A possible role of π-stacking in the self-assembly of amyloid fibrils. *FASEB. J.* 16:77–83.

Ghadiri, M. R., J. R. Granja, R. A. Milligan, D. E. McRee, and N. Khazanovich. 1993. Self-assembling organic nanotubes based on a cyclic peptide architecture. *Nature.* 366:324–327.

Goormaghtigh, E., V. Cabiaux, and J. M. Ruysshaert. 1994. Determination of soluble and membrane protein structures by Fourier transform infrared spectroscopy: I. Assignments and models compounds. *In* Subcellular Biochemistry: Physicochemical Methods in the Study of Biomembranes. H. J. Hillerson and C. B. Rabston, editors. Plenum Press, New York. 329–362.

Grabielle-Madelmont, C., and R. Perron. 1983. Calorimetric studies on phospholipid-water systems. II. Study of water behavior. *J. Colloid Interface Sci.* 95:483–493.

Haris, P. I., and D. Chapman. 1995. The conformational analysis of peptides using Fourier transform IR spectroscopy. *Biopolymers.* 37:251–263.

Hartgerink, J. D., E. Beniash, and S. I. Stupp. 2002. Peptide-amphiphile nanofibers: a versatile scaffold for the preparation of self-assembling materials. *Proc. Natl. Acad. Sci. USA.* 99:5133–5138.

Hatakeyama, H., and T. Hatakeyama. 1998. Interaction between water and hydrophilic polymers. *Thermochim. Acta.* 308:3–22.

Hitt, A. L., A. R. Cross, and R. C. Williams, Jr. 1990. Microtubule solutions display nematic liquid-crystalline structure. *J. Biol. Chem.* 265:1639–1647.

Holmes, K. C., D. Popp, W. Gebhard, and W. Kabsch. 1990. Atomic model of the actin filament. *Nature.* 347:44–49.

Kleman, M. 1980. Developable domains in hexagonal liquid crystals. *J. Phys.-Paris.* 41:737–745.

Klug, A. 1983. From macromolecules to biological assemblies (nobel lecture). *Angew. Chem. Int. Edit.* 22:565–636.

Krimm, S., and J. Bandekar. 1986. Vibrational spectroscopy and conformation of peptides, polypeptides, and proteins. *Adv. Protein Chem.* 38:181–364.

Langer, R. 2001. Drugs on target. *Science.* 293:58–59.

Lehn, J.-M. 2002. Toward complex matter: supramolecular chemistry and self-organization. *Proc. Natl. Acad. Sci. USA.* 99:4763–4768.

Li, H., and G. J. Thomas, Jr. 1991. Cysteine conformation and sulfhydryl interactions in proteins and viruses. 1. Correlation of the Raman S-H band with hydrogen bonding and intramolecular geometry in model compounds. *J. Am. Chem. Soc.* 113:456–462.

Paternostre, M., M. Viard, O. Meyer, M. Ghanam, M. Ollivon, and R. Blumenthal. 1997. Solubilization and reconstitution of vesicular stomatitis virus envelope using octylglucoside. *Biophys. J.* 72:1683–1694.

Mattioli, T. A., J. C. Williams, J. P. Allen, and B. Robert. 1994. Changes in primary donor hydrogen-bonding interactions in mutant reaction centers from *Rhodobacter sphaerödes*: identification of all the conjugated carbonyl groups. *Biochemistry.* 33:1636–1643.

Namba, K., and G. Stubbs. 1986. Structure of tobacco mosaic virus at 3.6 A resolution: implications for assembly. *Science.* 231:1401–1406.

Narayanan, T., O. Diat, and P. Boesecke. 2001. SAXS and USAXS on the high brilliance beamline at the ESRF. *Nucl. Instrum. Meth. A.* 465:1005–1009.

Nogales, E., and Y. F. Inclan. 2000. Structural models for the self-assembly and microtubule interactions of γ-, δ- and ε-tubulin. *J. Cell Sci.* 114: 413–422.

Nogales, E., S. G. Wolf, and K. H. Downing. 1998. Structure of the $\alpha\beta$ tubulin dimer by electron crystallography. *Nature.* 391:199–203.

Oster, G., and D. P. Riley. 1952. Scattering from cylindrically symmetric systems. *Acta Crystallogr.* 5:272–276.

Pott, T., M. Paternostre, and E.-J. Dufourc. 1998. A comparative study of the action of melittin on sphingomyelin and phosphatidylcholine bilayers. *Eur. Biophys. J.* 27:237–245.

Privalov, P. L. 1980. Heat capacity study in biology. *In* Biological Microcalorimetry. A. E. Beezer, editor. Academic Press, London and New York. 413–451.

Serpell, L. C. 2000. Alzheimer's amyloid fibrils: structure and assembly. *Biochim. Biophys. Acta.* 1502:16–30.

Serpell, L. C., P. E. Fraser, and M. Sunde. 1999. X-ray fiber diffraction of amyloid fibrils. *Methods Enzymol.* 209:526–536.

Sugeta, H., A. Go, and T. Miyazawa. 1973. Vibrational spectra and molecular conformations of dialkyl disulfides. *Bull. Chem. Soc. Jpn.* 46:3407–3411.

Sunde, M., and P. Blake. 1997. The structure of amyloid fibrils by electron microscopy and X-ray diffraction. *Adv. Protein Chem.* 50:123–159.

Thamann, T. J. 1998. Raman spectroscopic studies of a dimeric form of recombinant bovine growth hormone. *Anal. Biochem.* 265:202–207.

Valéry, C., M. Paternostre, B. Robert, T. Gulik-Krzywicki, J.-C. Dedieu, G. Keller, T. Narayanan, M.-L. Torres, R. Cherif-Cheikh, P. Calvo, and F. Artzner. 2003. Biomimetic organization: octapeptide self assembly into nanotubes of viral capsid like dimension. *Proc. Natl. Acad. Sci. USA.* 100:10258–10262.

Vauthey, S., S. Santoso, H. Gong, N. Watson, and S. Zhang. 2002. Molecular self-assembly of surfactant-like peptides to form nanotubes and nanovesicles. *Proc. Natl. Acad. Sci. USA.* 99:5355–5360.

Venyaminov, S. Y., and N. N. Kalnin. 1990. Quantitative IR spectrophotometry of peptide compounds in water (H2O) solutions. II. Amide absorption bands of polypeptides and fibrous proteins in a-, b-, and random coil conformations. *Biopolymers.* 30:1259–1271.

Vohnik, S., C. Hanson, R. Tuma, J. A. Fuchs, C. Woodward, and G. J. Thomas, Jr. 1998. Conformation, stability, and active-site cysteine titrations of *Escherichia coli* D26A thioredoxin probed by Raman spectroscopy. *Protein Sci.* 7:193–200.

Walsh, D. M., D. M. Hartley, Y. Kusumoto, Y. Fezoui, M. M. Condron, A. Lomakin, G. B. Benedk, D. J. Selkoe, and D. B. Teplow. 1999. Amyloid β-protein fibrillogenesis : structure and biological activity of protofribriller intermediates. *J. Biol. Chem.* 274:25945–25952.

Whitesides, G. M., and M. Boncheva. 2002. Beyong molecules: self assembly of mesoscopic and macroscopic components. *Proc. Natl. Acad. Sci. USA.* 99:4769–4774.

Zhang, S. 2003. Fabrication of novel biomaterials through molecular self-assembly. *Nat. Biotechnol.* 21:1171–1178.